Journal of Alloys and Compounds 507 (2010) 151–156

Contents lists available at ScienceDirect

Journal of Alloys and Compounds

journal homepage: www.elsevier.com/locate/jallcom

# Influence of copper substitution on structural, electrical and dielectric properties of $Ni_{(1-x)}Cu_xMn_2O_4$ ($0 \le x \le 1$) ceramics

R.N. Jadhav, Vijaya Puri*

*Thick and Thin Film Device Lab, Department of Physics, Shivaji University, Kolhapur 416004, Maharashtra, India*

ARTICLE INFO

*Article history:*
Received 20 March 2010
Received in revised form 17 July 2010
Accepted 20 July 2010
Available online 30 July 2010

*Keywords:*
NTC ceramics
Nickel manganite
Electrical properties
Dielectric properties

ABSTRACT

Copper substituted polycrystalline nickel manganite viz. $Ni_{(1-x)}Cu_xMn_2O_4$ ($0 \le x \le 1$) ceramics were prepared by oxalate process. The replacement of nickel by copper plays an important role in changing the lattice parameter, X-ray density, sintered density, porosity, grain size, DC resistivity at different temperatures, drift mobility and dielectric properties at different frequencies. The lattice parameter and crystallite size decreases with increase in copper content. The addition of copper promotes grain growth, decrease in porosity and increase in sintered density. The room temperature DC electrical resistivity decreases from 43.50 to 32.92 MΩ cm and dielectric constant increases from $\sim 2 \times 10^3$ to $3 \times 10^5$ at low frequency (20 Hz) as copper concentration increases.



## 1. Introduction

Low cost, ease of manufacturing and interesting thermistor properties make polycrystalline nickel manganite ($NiMn_2O_4$) one of the most important materials today and widely used as a material for Negative Temperature Coefficient (NTC) thermistors [1–3]. The cubic spinel structure, has a structural formula $AB_2O_4$ based on the cubic close packing of oxygen ions in which cations are situated on both tetrahedral (A sites) and octahedral (B sites) [4,5]. The nickel manganites also crystallizes in such cubic spinal structures. The mechanism responsible for conduction in nickel manganite is phonon assisted electron jumping (hopping) between $Mn^{3+}$ and $Mn^{4+}$ cations occupying octahedral sites [6]. The symmetry of the spinel structure as well as the site occupation is strongly dependent on the 3d transition metals used for the synthesis of the ceramic and also on the manufacturing conditions and there are some reports available describing the structural and electrical properties of nickel manganite [7,8]. As nickel manganite is a good NTC thermistor, most of the researchers concentrate only on the electrical properties of this material and not much work has been done on dielectric properties of this material. There are some reports available on the study of the effect of copper and zinc on ferrite [9–11] but very few reports are available to study the effect of copper on the dielectric properties of manganite. Copper plays an important role in the physical and electrical properties of nickel manganite [12]. This research is undertaken to study the effect of substitution of copper on the physical, electrical and dielectric properties of $Ni_{(1-x)}Cu_xMn_2O_4$ ($0 \le x \le 1$) ceramic.

The physical and electrical properties of materials with different concentrations strongly depend on their microstructural properties. It is also useful to understand the relationship between their processing parameter as well as their behavior when used in practical applications. Changes due to variation of copper concentration in nickel manganite on the lattice parameter, X-ray density, sintered density, porosity, grain size, DC electrical resistivity, thermistor constant, activation energy and dielectric constant have been discussed in this work.

### 2. Experimental details

The $Ni_{(1-x)}Cu_xMn_2O_4$ ($x = 0.0$, 0.2, 0.4, 0.6, 0.8, 1.0) was prepared by oxalate process employing nickel acetate [$Ni(CH_3COO)4H_2O$], manganese acetate [$Mn(CH_3COO)4H_2O$], cupric acetate [$Cu(CH_3COO)4H_2O$] and oxalic acid as starting materials. 0.5 M solution of nickel, manganese, and copper acetate was prepared and added drop wise to 2 M hot (75 °C) oxalic acid solution with constant stirring. After cooling to room temperature the precipitate was filtered, washed with distilled water and dried. The prepared powder was dried at room temperature, pre-sintered at 350 °C for 3 h and mixed with PVA (polyvinyl alcohol) binder. The powder was pressed into small disk of 1.5 cm diameter and ~0.2 cm thickness under a pressure of 10 Ton for 1–2 min. The pellets were sintered at temperature 1000 °C in a muffle furnace for 8 h followed by cooling. The structure of $Ni_{(1-x)}Cu_xMn_2O_4$ ($x = 0.0$–1.0) was confirmed by XRD Phillips PW 3710 diffractometer using Cu Kα radiation ($\lambda = 1.541838$ Å). The crystal structure and the density related parameter of the samples were determined from the XRD data. The microstructure was examined using scanning electron microscopy (SEM JSM-6360 JEOL, Japan). The DC electrical resistivity ($\rho$) for all the different compositions were measured by two-probe method. As nickel manganite is a good NTC thermistor most of the researchers concentrate only on the DC electrical properties of this material and not much work has been done

* Corresponding author. Fax: +91 231 2691533.
*E-mail address:* vrp_phy@unishivaji.ac.in (V. Puri).

0925-8388/$ – see front matter © 2010 Elsevier B.V. All rights reserved.
doi:10.1016/j.jallcom.2010.07.143

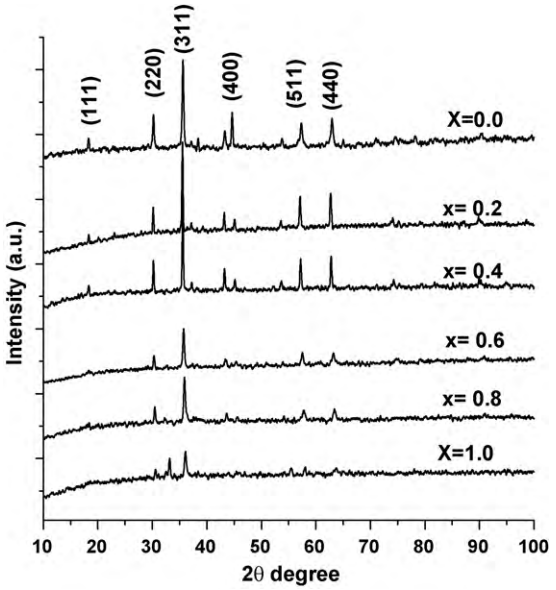


**Fig. 1.** X-ray diffraction pattern of $Ni_{(1-x)}Cu_xMn_2O_4$ ($0 \le x \le 1$) ceramic.

on AC dielectric properties of this material. The commercially available LCR meter bridge (HP 4284A) in the frequency region 20 Hz to 1 MHz at room temperature was used for this measurement.

## 3. Results and discussion

### 3.1. XRD studies

The spinel structure with predominant (3 1 1) plane of $Ni_{(1-x)}Cu_xMn_2O_4$ ($0 \le x \le 1$) ceramic was confirmed from X-ray spectrum as shown in Fig. 1. These patterns confirm the formation of single cubic phase. The average crystallite size for the different compositions was calculated by Debye Sherrer's formula [13]. It was found that the crystallite size decreased from ~27 to 19.5 nm with copper content. The lattice parameter decreased continuously with increase in copper concentration from 8.38 to 8.24 Å which is tabulated in Table 1. The decrease in lattice constant and crystallite size with increase in copper content is due to the smaller ionic radii of $Cu^{2+}$ (0.70 Å) as compared to those replaced $Ni^{2+}$ (0.78 Å) [14]. A partial replacement of $Ni^{2+}$ with $Cu^{2+}$ causes the shrinkage of the unit cell dimensions resulting in decrease in the lattice parameter.

#### 3.1.1. X-ray density

The X-ray density ($\rho_x$) was calculated by the formula [15]:

$$\rho_x = \frac{8M}{Na^3}$$

where '*M*' is the molecular weight of composition, '*N*' is the Avogadro's number and '*a*' is the lattice parameter.

The obtained X-ray densities for all the six compositions are tabulated in Table 1. It was observed that the X-ray density increased with increase in copper concentration from 5.23 to 5.62 g/cm$^3$. It can be explained on the basis of Cu atom being heavier than the replaced Ni and leading to the increase in weight and also the X-ray density being inversely proportional to the lattice constant [16,17], as also seen from Table 1.

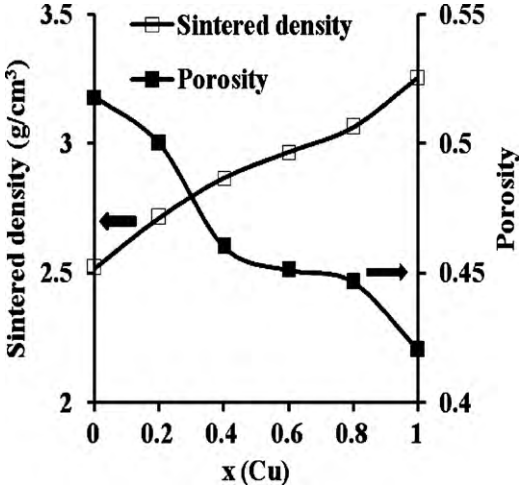


**Fig. 2.** Variation of sintered density (g/cm$^3$) and porosity with $x$ (Cu) in $Ni_{(1-x)}Cu_xMn_2O_4$ ceramic.

#### 3.1.2. Sintered density

The sintered density ($\rho_s$) was calculated using the formula [15]:

$$\rho_s = \frac{m}{\pi r^2 h}$$

where '*m*' is the mass of the pellet. '*r*' is the radius of the pellet and '*h*' is the thickness of the pellet.

The calculated sintered density with copper concentration is shown in Fig. 2. The sintered density increased linearly with increase in Cu concentration from 2.52 to 3.26 g/cm$^3$. This increase may be attributed to (i) acceleration of cation interdiffusion due to Cu ions and (ii) the increase in the reactivity of the fine manganite grains which coalesce to form bigger grains leading to pore reduction and volume shrinkage [18].

It was observed that X-ray density of each composition is larger than the corresponding sintered density. This is may be due to the existence of pores in the prepared samples.

#### 3.1.3. Porosity

The porosity ($P$) for different compositions was calculated by the relation:

$$P = 1 - \frac{\rho_s}{\rho_x}$$

where $\rho_s$ and $\rho_x$ are defined above.

The variation of sintered density and porosity related to copper concentration is also shown in Fig. 2. From the figure it is observed that with the increase in copper content porosity decreased linearly from 0.51 to 0.42, which should be expected because of the reasons stated above. As copper concentration increases the number

**Table 1**
Lattice parameter, X-ray density, grain size ($\rho_x$) and drift mobility ($\mu_d$) of $Ni_{(1-x)}Cu_xMn_2O_4$ ($0 \le x \le 1$) ceramic.

| Parameter | $x$(Cu) | | | | | |
|---|---|---|---|---|---|---|
| | $x=0.0$ | $x=0.2$ | $x=0.4$ | $x=0.6$ | $x=0.8$ | $x=1$ |
| Lattice parameter (Å) | 8.38 | 8.37 | 8.36 | 8.32 | 8.27 | 8.24 |
| X-ray density (gm/cm$^3$) | 5.23 | 5.25 | 5.32 | 5.41 | 5.54 | 5.62 |
| Grain size (μm) | 0.45 | 0.50 | 0.60 | 0.70 | 1.10 | 1.85 |
| Drift mobility (room temp.) ($\times 10^{-16}$ cm$^2$/V$^{-s}$) | 13.38 | 13.59 | 13.95 | 14.50 | 14.89 | 15.01 |

of pores is reduced due to increase in grain size as a result of which individual grains come closer to each other and the effective area of grain to grain contact increases. This in turn results in greater densification or lesser porosity which is observed from X-ray and sintered density and also in SEM images (Fig. 3).

### 3.2. Surface morphology

Representative micrographs for $Ni_{(1-x)}Cu_xMn_2O_4$ ($0 \leq x \leq 1$) are shown in Fig. 3. The surface morphology of all the compositions showed that the grain size increased with increase in copper concentration from 0.45 to 1.85 μm. The grain size has been tabulated in Table 1. The increase in grain size with copper content is due to the higher atomic mobility of copper ions induced by liquid phase sintering [19]. On substitution of copper the grain texture turns to polyhedral with lesser microstructure homogeneity and a variation in grains size is observed which gradually increases with increase in copper concentration. The grain size obtained in this work is much smaller than those for the samples prepared by ceramic method (3–18 μm) [20].

### 3.3. DC electrical resistivity

Fig. 4 shows the relationship between $\log \rho$ and $1000/T\,(K^{-1})$ for $Ni_{(1-x)}Cu_xMn_2O_4$ which follows the Arrhenius plot.

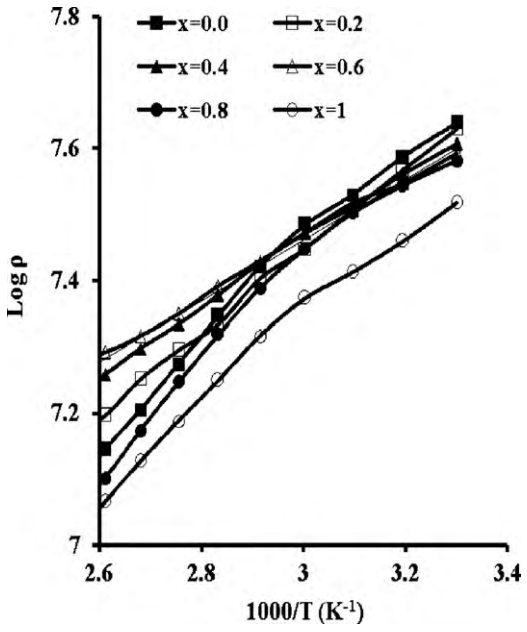


**Fig. 4.** Relationship between $\log \rho$ and $1000/T\,(K^{-1})$ for $Ni_{(1-x)}Cu_xMn_2O_4$ ($0 \leq x \leq 1$) ceramic.

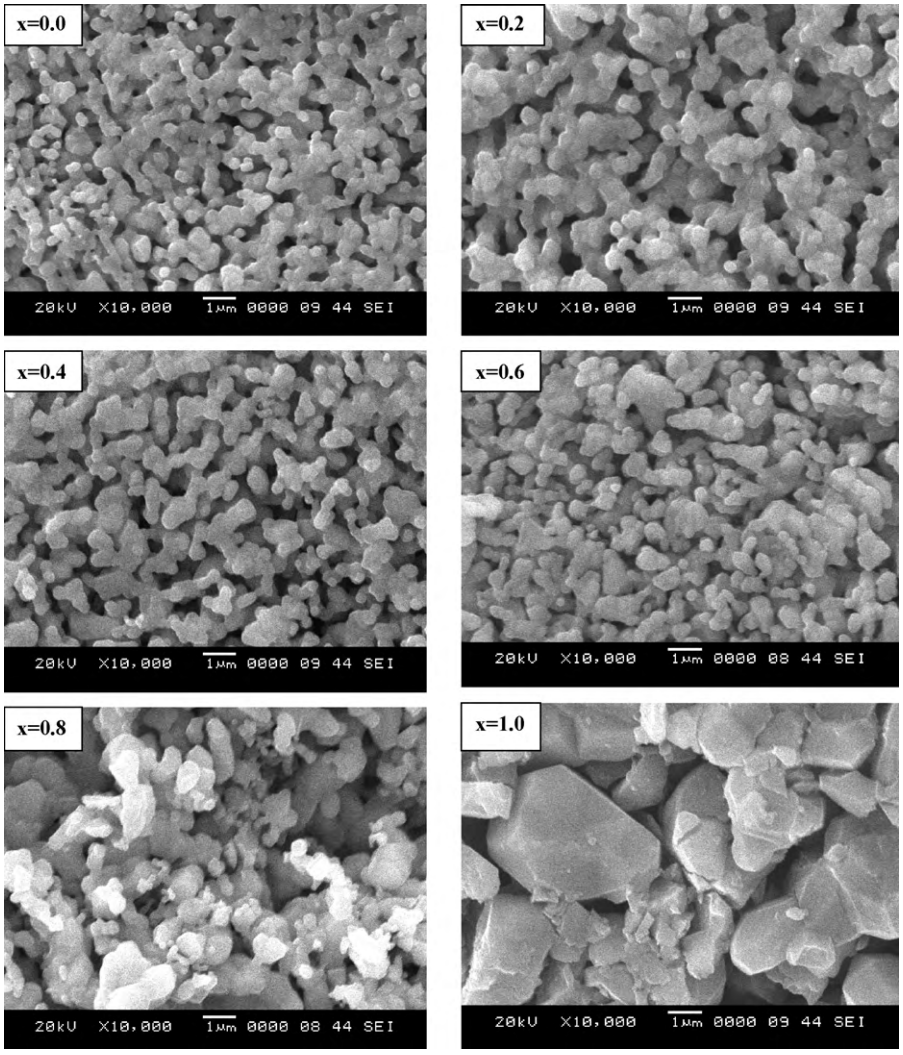


**Fig. 3.** SEM images of $Ni_{(1-x)}Cu_xMn_2O_4$ ($0 \leq x \leq 1$) ceramic.

**Table 2**
Composition dependent thermistor constant, activation energy, sensitivity index and stability factor of $Ni_{(1-x)}Cu_xMn_2O_4 (0 \le x \le 1)$ ceramic.

| Composition of thermistor | Resistivity at 30 °C (MΩ cm) | Resistivity at 90 °C (MΩ cm) | Thermistor constant $B$ (K) | Activation energy (eV) | | Sensitivity index ($\alpha$) | Stability factor (SF) |
|---|---|---|---|---|---|---|---|
| $NiMn_2O_4$ | 43.50 | 20.3 | 1397.36 | 0.1197 | | 0.0152 | 0.3309 |
| $Ni_{0.8}Cu_{0.2}Mn_2O_4$ | 42.09 | 21.04 | 1270.87 | 0.1036 | | 0.0138 | 0.3010 |
| $Ni_{0.6}Cu_{0.4}Mn_2O_4$ | 40.50 | 21.46 | 1164.04 | 0.1107 | | 0.0126 | 0.2757 |
| $Ni_{0.4}Cu_{0.6}Mn_2O_4$ | 39.18 | 19.59 | 1270.87 | 0.0976 | | 0.0138 | 0.3010 |
| | | | | Region I | Region II | | |
| $Ni_{0.2}Cu_{0.8}Mn_2O_4$ | 38.16 | 18.44 | 1333.03 | 0.1693 | 0.08366 | 0.0145 | 0.3157 |
| $CuMn_2O_4$ | 32.92 | 17.28 | 1484.74 | 0.1612 | 0.0954 | 0.0161 | 0.2798 |

The DC electrical resistivity of $Ni_{(1-x)}Cu_xMn_2O_4$ was found to decrease with the increase in copper concentration from 0.0 to 1.0 at room temperature. In nickel manganite the electrical conductivity does not depend only on the $Mn^{3+}$ and $Mn^{4+}$ concentration or hopping distance. For a given concentration of substituted transition metal ions, the configuration of ions in octahedral position also governs the conductivity. Indeed all the $Mn^{3+}$ ions do not participate in hopping process, to participate in hopping they need to have in their vicinity $Mn^{4+}$ ion. Therefore, the ordering between $Mn^{3+}$ and $Mn^{4+}$ and the presence of foreign ions on octahedral sites may disrupt the conduction [21]. The decrease in resistivity with increase in copper is due to the fact that Cu ions prefer the occupation of tetrahedral (A) sites and Ni ions prefer the occupation of octahedral (B) sites, while Mn ions partially occupy the A and B sites. On increasing Cu ion substitution (at A sites), Ni ion concentration (at B sites) will decrease. This leads to the migration of some Mn ions from A sites to B sites to substitute the reduction in Ni ion concentration at B sites. As a result the number of $Mn^{4+}$ ions at the B sites (which is responsible for conduction in manganite) increases. According to this mechanism the electrical resistivity of the material is inversely proportional to the concentration product of $Mn^{3+}$ and $Mn^{4+}$. Consequently, resistivity decreases as copper concentration increases [22,12]. The decrease in resistivity due to copper content may also be due to the participation of $Cu^{+}$ and $Cu^{2+}$ cations at octahedral sites in the hopping process whereby increasing cation transition probability of localized carriers at octahedral sites [3,12]. Resistivity is actually the result of the combined factors such as grain size, crystal structure, imperfections and microstructure homogeneity. The high room temperature resistivity obtained in this work can be attributed to smaller grain size of the samples. Small grains imply larger number of insulating grain boundaries and hence greater energy barrier to electron conduction resulting thereby in higher resistivity.

The resistivity at 30 and 90 °C, thermistor constant ($B_{30/90}$), activation energy, sensitivity index and stability factor are tabulated in Table 2.

The thermistor constant $B_{30/90}$ was calculated by the equation [21]:

$$B_{30/90} = \frac{\ln(R_{30}/R_{90})}{[(1/T_{30}) - (1/T_{90})]}$$

where $R_{30}$ and $R_{90}$ are resistivity measured at 30 and 90 °C respectively.

The activation energy was calculated using the equation $E = 2.303{*}K{*}$ slope of $\log\rho$ vs. $1000/T$ ($K^{-1}$) curve. The sensitivity index ($\alpha$) and stability factor (SF) were calculated using the following formula [23]:

$$\alpha = \frac{-B}{T^2}, \quad SF = \log\frac{R_{max}}{R_{min}}$$

The $Ni_{(1-x)}Cu_xMn_2O_4$ NTC ceramics shows the coefficient of temperature sensitivity in the range ~1300 K which is in the industrial range.

The activation energy is primarily the energy for hopping process from a cation $M^{n+}$ to $M^{(n+1)}$ on the octahedral sites and hence the mobility of the cations [3]. It is well known that conduction is caused in nickel manganite by hopping of electron between $Mn^{3+}$ and $Mn^{4+}$ on octahedral sites. The activation energies calculated using the Arrhenius equation and from the specific resistivity values are tabulated in Table 2. The Arrhenius plot shows two distinct regions with different slopes for two compositions $x = 0.8$ and $x = 1.0$. Generally the change in slope is attributed to a change in conduction mechanism. The conduction at low temperature is due to the hopping of electrons between $Mn^{3+}$ and $Mn^{4+}$ ions whereas at high temperature it is due to polaron hopping. The activation energies show direct response to the changes in concentration of copper substitution in nickel manganite because the substitution could change the energy band structure of the compound. The equation infers that the current carriers are generally electrons originated from $Mn^{3+}$ centers, which acts as electron donor. At higher temperatures the concentration of $Mn^{3+}$ ions increases along with increased hopping of holes generated from $Ni^{3+}$ and $Ni^{2+}$ ions transition. Similar results have been observed by Balaji et al. [24] in tin substituted nickel ferrite.

Drift mobility ($\mu_d$) of the all six compositions has been calculated by using the relation given by Ajmal et al. [15]. Drift mobility of all the six compositions at room temperature are tabulated in Table 1. It increases from $13.38 \times 10^{-16}$ to $15.01 \times 10^{-16}$ $cm^2/V^{-s}$ with concentration of copper varying from 0.0 to 1.0. It can be seen that the compositions having higher resistivity have low mobility and vice versa [25].

### 3.4. Dielectric constant

The dielectric constant ($\varepsilon'$) was determined by the well known relation:

$$\varepsilon' = \frac{Cd}{\varepsilon_0 A}$$

where '$C$' is the capacitance of the pellet in Farad, '$d$' is the thickness of the pellet in meter, '$A$' is the cross sectional area of the flat surface pellet, and '$\varepsilon_0$' is the constant of permittivity for free space.

Silver paint (air dried) was coated on the flat surfaces to form electrodes for dielectric measurements. The dielectric constant of the samples was calculated from the capacitance ($Cp$) and loss factor ($\tan\delta$) values measured using LCR meter bridge (HP4284A) in the frequency range 20 Hz to 1 MHz at room temperature. The compositional variation of dielectric constant ($\varepsilon'$) and loss factor ($\tan\delta$) with frequency (20 Hz to 1 MHz) at room temperature is shown in Figs. 5 and 6 respectively. It shows that the value of dielectric constant at lower frequency (20 Hz) is much higher, for $NiMn_2O_4$ it is $\sim 2 \times 10^3$ and $3 \times 10^5$ for $CuMn_2O_4$. It decreases with frequency and becomes constant at higher frequency, attaining a value of $\sim 0.18 \times 10^3$ for $NiMn_2O_4$ and $\sim 2.991 \times 10^3$ for $CuMn_2O_4$. The mechanism of polarization in polycrystalline manganite is mainly reported due to the electron exchange interaction (hopping) between the $Mn^{3+}$ and $Mn^{4+}$ ions at the octahedral sites. This elec-

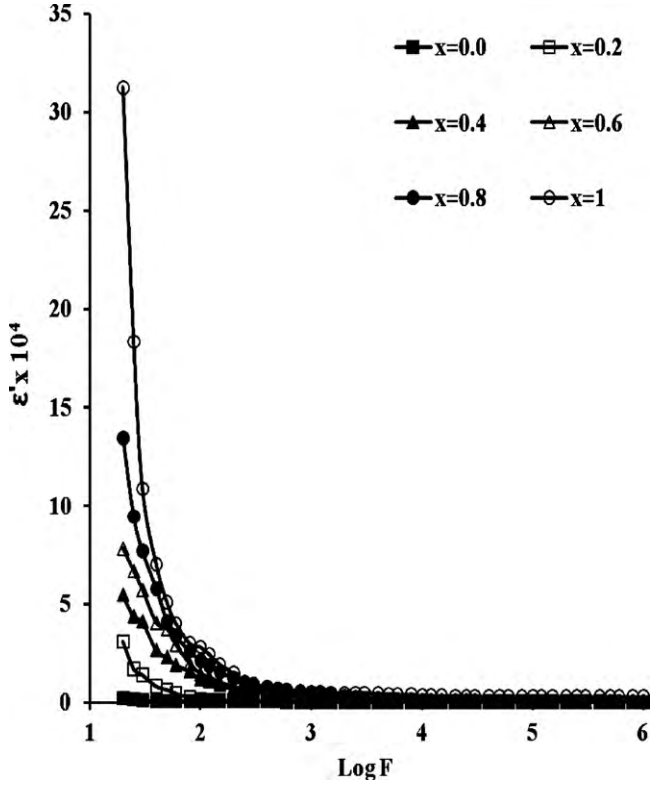


**Fig. 5.** Variation of dielectric constant with frequency of $Ni_{(1-x)}Cu_xMn_2O_4$ ($0 \le x \le 1$) ceramic.

tron hopping appears to be favourable at lower applied ac electric field frequencies; the dielectric constant has therefore a maximum value at lower frequencies [26]. The variation of dielectric constant with frequency can be explained according to space charge polarization of Maxwell and Wagner two layer model with Koop's phenomenological theory. According to this model the dielectric structure of the ceramic material is considered to be made up of two layers. The first layer consists of conducting grains and the second layer consists of poorly conducting grain boundaries. At lower frequencies the electrons at grain boundaries are more active than those in the grains, while at higher frequencies only the electrons in grains are active in electrical conduction. The electronic exchange between $Mn^{3+}$ and $Mn^{4+}$ is due to the local movement of electrons in the direction of electric field which determines the polarization in manganite. Polarization decreases with increase in frequency and then attains a constant value. It is because at higher frequencies the electrons exchange $Mn^{3+} \leftrightarrow Mn^{4+}$ cannot follow the applied ac electric field hence $\varepsilon'$ and $\tan\delta$ decreases [27]. The decreasing trend in $\varepsilon'$ with increase in frequency is natural due to the fact that any species that contribute to polarizability is found to lag behind the applied field at higher frequencies.

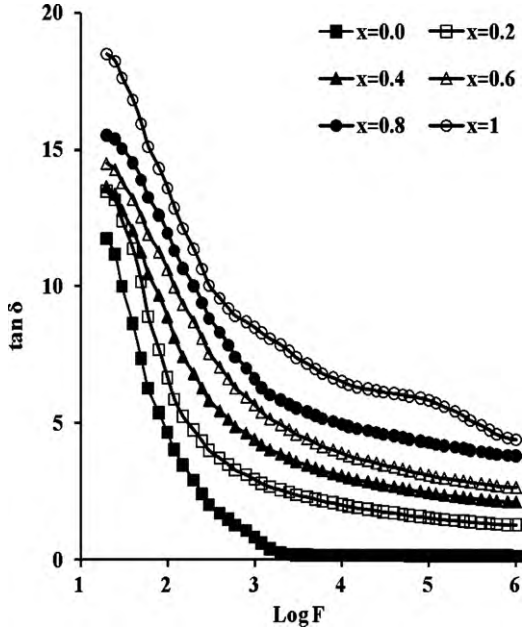


**Fig. 6.** Variation of loss factor with frequency of $Ni_{(1-x)}Cu_xMn_2O_4$ ($0 \le x \le 1$) ceramic.

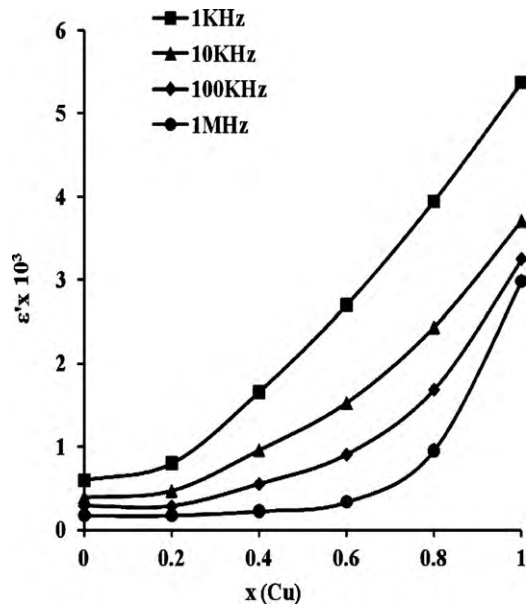


**Fig. 7.** Dielectric constant as a function of $x$(Cu) in $Ni_{(1-x)}Cu_xMn_2O_4$ ceramic.

The variations of dielectric constant with copper concentration in $Ni_{(1-x)}Cu_xMn_2O_4$ ($0 \le x \le 1$) ceramics shown in Fig. 7. It is observed that as copper content increased dielectric constant also increased. The polarization is affected by some factors such as structural homogeneity, stoichiometry, density, grain size and porosity of the sample. The higher density of these compositions (when copper concentration increases) implies, decrease in the porosity and higher number of polarizing species per unit volume, both contributing to the observed increase in polarization [14]. When copper concentration increases in nickel manganite it results in a decrease in structural homogeneity of the manganite which may cause increase in polarization.

## 4. Conclusions

We conclude on the basis of the experimental results that the substitution of copper in $Ni_{(1-x)}Cu_xMn_2O_4$ ceramics produce appreciable changes in the structural and electrical properties. Grain size and sintered density increased linearly with copper content and porosity decreased. The resistivity decreased linearly with copper and low activation energy obtained. The good value of thermistor constant ($B$), make these compounds promising for high temperature NTC type thermistor applications, with tunable range of sensitivity.

The dielectric constant of $0.6 \times 10^3$ to $5.3 \times 10^3$ at a frequency of 1 kHz and $0.18 \times 10^3$ to $2.99 \times 10^3$at a frequency of 1 MHz was obtained with increase in copper concentration. The value of dielectric constant increased from $2 \times 10^3$ to $3 \times 10^5$ at room temperature

for frequency 20 Hz when copper was substituted in nickel manganite. The high dielectric constant might be used in capacitors of dynamic random access memories (DRAM) for personal computers and workstations. The results obtained in this work strongly suggests that $Ni_{(1-x)}Cu_xMn_2O_4$ ($0 \leq x \leq 1$) ceramics can be a good candidate for applications where high dielectric constant with low loss in radio-frequency range are required. Copper content has significant influence on the electromagnetic properties, such as initial permittivity, quality factor, DC resistivity, dielectric constant and dielectric loss tangent as well as their frequency dispersion for Ni–Cu manganite and it can be applicable in temperature-compensating dielectrics at room temperature.

These ceramics might also be attractive for capacitor applications and certainly for microelectronics, microwave devices (like mobile phones), where the miniaturization of the devices is crucial.

## Acknowledgment

One of the authors Vijaya Puri gratefully acknowledges the UGC India for Award of Research Scientist 'C'.

## References

[1] K. Park, J. Lee, S. Kim, W. Seo, W. Cho, C. Lee, S. Nahm, J. Alloys Compd. 467 (2009) 310–316.
[2] S.A. Kanade, V. Puri, J. Alloys Compd. 475 (2009) 352–355.
[3] K. Park, J. Am. Ceram. Soc. 88 (2005) 862–866.
[4] C. Zhao, B. Wang, P. Yang, L. Winnubst, C. Chen, J. Eur. Ceram. Soc. 28 (2008) 35–40.
[5] R. Kambale, N. Adhate, B. Chougule, Y. Kolekar, J. Alloys Compd. 491 (2010) 372–377.
[6] K. Park, J. Lee, J. Alloys Compd. 475 (2009) 513–517.
[7] S. Kanade, V. Puri, Mater. Res. Bull. 43 (2008) 819–824.
[8] S.M. Savic, M.V. Nikolic, O.S. Aleksic, M. Slankamenac, M. Zivanov, P.M. Nikolic, Sci. Sin. 40 (2008) 27–32.
[9] S. Mazen, A. Taher, J. Alloys Compd. 498 (2010) 19–25.
[10] M. Gabal, Y. Angari, S. Al-Juaid, J. Alloys Compd. 492 (2010) 411–415.
[11] H. Hsianga, L. Meia, C. Hsib, Y. Liua, F. Yena, J. Alloys Compd. 502 (2010) 163–168.
[12] A.V. Salker, S.M. Gurav, J. Mater. Sci. 35 (2000) 4713–4719.
[13] P.P. Hankare, M.R. Kadam, P.D. Kamble, S.D. Jadhav, U.B. Sankpal, R.P. Patil, V.B. Helavi, N.S. Gajbhiye, J. Alloys Compd. 489 (2010) 233–236.
[14] M. Dimri, A. Verma, S. Kashyap, D. Dube, O. Thakur, C. Prakash, Mater. Sci. Eng. B 133 (2006) 42–48.
[15] M. Ajmal, A. Maqsood, Mater. Sci. Eng. B 139 (2007) 164–170.
[16] Q. Wei, J. Lie, Y. Chen, J. Mater. Sci. 36 (2001) 5115–5118.
[17] U. Ghazanfara, S.A. Siddiqia, G. Abbas, Mater. Sci. Eng. B 118 (2005) 84–86.
[18] A.C.F.M. Costa, E. Tortella, M.R. Morallie, R.H.G.A. Kiminani, J. Mag. Mag. Mater. 256 (2003) 174–182.
[19] E. Rezlescu, L. Sachelarie, P.D. Popa, N. Rezlescu, IEEE Trans. Mag. 36 (2000) 3962–3967.
[20] K. Park, D. Bang, J. Mater. Sci. Mater. Electron. 14 (2003) 81–87.
[21] S.A. Kanade, V. Puri, Mater. Lett. 60 (2006) 1428–1431.
[22] E. Lbadraroui, E. Baudour, J. Bouree, F. Gillot, B. Fritsch, S. Rousset, Solid State Ionics 93 (1997) 219–225.
[23] S. Jagtap, S. Rana, U. Mulik, D. Amalanekar, Microelectron. Int. 24 (2007) 7–13.
[24] S. Balaji, J. Kalai Selvan, L. John Bechmans, S. Angappan, K. Subramanian, C.O. Augustin, Mater. Sci. Eng. B 119 (2005) 119–124.
[25] U. Ghazanfar, S.A. Siddiqi, G. Abbas, Mater. Sci. Eng. B 118 (2005) 132–134.
[26] M. Iqbal, Z. Ahmed, J. Power Sources 179 (2008) 763–769.
[27] S. Angappan, L.J. Berchmans, C.O. Augustin, Mater. Lett. 58 (2004) 2283–2289.